Tube number density control of carbon nanotubes on anodic aluminum oxide template

Po-Lin Chen, Jun-Kai Chang, Fu-Ming Pan, Cheng-Tzu Kuo*

Department of Materials Science and Engineering, National Chiao Tung University, Hsinchu, Taiwan

Available online 3 February 2005

Abstract

We demonstrate that the tube number density of well-aligned carbon nanotubes (CNTs) grown over the nanoporous anodic aluminum oxide (AAO) template can be directly controlled by adjusting the CH_4/H_2 feed ratio during the CNT growth in a microwave plasma electron cyclotron resonance chemical vapor deposition (ECR-CVD) system. During the CNT growth, the nanotube growth and the amorphous carbon deposition on the AAO pore wall take place simultaneously. The amorphous carbon sediment will gradually cover up the AAO nanopores and prevent the nanotubes to grow out of the nanopores. By adjusting the CH_4/H_2 feed ratio, one can control the amount of the deposited amorphous carbon and thus the number of CNTs grown over the AAO nanopores. It was found that the CNT density decreases linearly with increasing the CH_4 concentration. The CNT density decreased by a factor of about 4.5 when the CH_4 concentration increased from 9% to 91%.
© 2004 Elsevier B.V. All rights reserved.

Keywords: Carbon nanotubes; Amorphous carbon; Density control; Plasma CVD

1. Introduction

Carbon nanotubes (CNTs) have attracted much interest for their remarkable properties and diversified applications since they were discovered by Iijima [1]. In particular, CNTs have become one of the most promising candidates for future generations of cold-cathode flat panel displays and various vacuum microelectronic devices because of their excellent field emission properties, i.e., good emission stability, long emitter lifetime, and relatively low threshold voltage [2–4]. For the practical application in field emission displays (FEDs), it is necessary to grow vertically aligned CNT arrays on a large area with suitable tube number density and tube dimensions. In recent years, template methods, especially anodic aluminum oxide (AAO) nanoporous templates, have been widely introduced to produce well aligned and dispersed CNT arrays [5–8]. Nanoporous AAO, which consists of vertical pore channel arrays with a hexagonal packing structure, was obtained by electrochemical anodization of aluminum in an acidic electrolyte [9,10]. By adjusting the anodizing conditions, one can control the diameter, the length, and the density of nanopores, making AAO an ideal template for fabricating ordered arrays of nanostructured materials.

As the AAO is used as the template to grow CNTs without the catalyst, the diameter, the length, the arrangement, and the packing density of aligned nanotubes can faithfully replicate the pattern of the AAO nanopore structure. However, the obtained tubes are very poor in graphitization [11,12]. When the transition metal catalyst is predeposited at the AAO pore bottom for the CNT growth, the crystallinity of the metal-catalyzed tubes can be appreciably improved, but the relatively high tube growth rate will lead to overgrowth and entanglement of the dense tubes [13,14]. For such a high density CNT array, the significant electrostatic screening effect caused by the proximity of neighboring tubes would reduce the field

enhancement and thus the emitted current [15]. In order to alleviate the screening effect, the nanotubes with a lower tube number density is favorable. Several methods such as electron-beam lithography [16], microcontact printing [15], shadow mask [17], and pulse–current electrochemical deposition [18], etc. have been proposed to control the catalyst site density aiming at the reduction of the CNT density. However, only a few research focus on the control of the tube number density of CNTs grown on AAO templates [19]. In this article, we report a simple and reliable method to control the CNT density on the AAO template by regulating the flow rate ratio of methane (CH_4) and hydrogen (H_2) precursor gases during the CNT growth. It was found that the tube number density of the aligned CNT arrays decreases linearly with increasing the CH_4 concentration.

2. Experimental

Fabrication of the nanoporous AAO template began with the deposition of a 6-μm-thick Al film on the p-Si (100) wafer by thermal evaporation. The two-step anodization was introduced to produce ordered pore channel arrays of AAO [20,21]. Anodization was first carried out in a 0.3-M oxalic acid solution at 21 °C under a constant polarization voltage of 40 V for 30 min. The resulting nanoporous AAO was then removed by wet chemical etching at 60 °C with a mixed solution of H_3PO_4 and CrO_3. The anodization was performed again under the conditions as the first step for 5 min. At the end of the second anodization, the voltage was dropped gradually from 40 to 10 V by 1 V steps in order to reduce the thickness of insulating alumina barrier under the pore bottom. After the voltage drop process, the nanopore was widened in a 5% H_3PO_4 solution for 1 h, and the alumina barrier was completely removed under this step. The cobalt catalyst for CNT growth was electrochemically deposited at the pore bottom in an electrolyte of 5% $CoSO_4 \cdot 7H_2O$ and 2% H_3BO_3 by applying an AC voltage 12.3 V_{rms} for 1 min.

The CNT growth was carried out in the microwave plasma electron cyclotron resonance chemical vapor deposition (ECR-CVD) system under 875-Gauss magnetic field strength. The gas mixture of CH_4 and H_2 was used as the carbon source. The total gas flow rate was kept at 22 sccm. The other growth conditions were the microwave power, 700 W; the substrate bias, −150 V; the working pressure, 0.25 Pa; the growth temperature, 600 °C; and the growth time, 30 min. The CH_4 concentration in the gas precursor was varied from 9% to 91% in order to investigate the influence of the CH_4/H_2 ratio on the CNT growth. The morphology and microstructure of the as-grown CNTs were characterized by field-emission scanning electron microscopy (FE-SEM; Hitachi S-4000) and transmission electron microscopy (TEM; JEOL JEM-2010F). The Auger chemical analysis was performed using a VG Microlab 310F Auger

system with a Schottky field emission electron source. The structural characterization of the samples was studied by Raman spectroscopy. Unpolarized visible Raman spectra were excited with the 632.8 nm line of a He–Ne laser and measured with the Jobin Yvon LABRAM HR Micro-Raman system.

3. Results and discussion

Fig. 1 shows the top-view SEM image of the as-prepared nanoporous AAO film produced by the two-step anodization. The self-organized nanopores with a uniform size distribution have a pore diameter about 60 nm, an interpore distance about 100 nm, and a pore density about 1.1×10^{10} pores/cm^2. The depth of the straight cylindrical pores is about 740 nm. The inset in Fig. 1 is the cross-sectional view of the AAO film after the Co electroplating. It is obvious that uniform Co particles were deposited at the AAO pore bottom. Fig. 2 shows the side-view SEM images of the Co-catalyzed CNTs on the AAO template grown at different CH_4 concentrations. The SEM observation of these samples exhibits that the CNT density significantly relies on the CH_4/H_2 feed ratio. Following the increase of the carbonaceous gas content, the number of nanotubes grown over the AAO nanopores decreases gradually. At the CH_4 concentration of 9% (see Fig. 2a), the tube number density of CNT is as high as 9.0×10^9 tubes/cm^2, indicating a tube filled ratio in pores of about 82%. In an extremely high CH_4 concentration of 91% (see Fig. 2c), the observed tube number density decreases significantly to about 2.0×10^9 tubes/cm^2, corresponding to tube filled ratio of about 18%. These figures also reveal that the nanotubes confined by the AAO nanopores are uniform in diameter and tend to be vertically aligned. Fig. 3 is the high-resolution TEM (HRTEM) image of the nanotube shown in Fig. 2b. Because the tube has a relatively large diameter, only a part of the
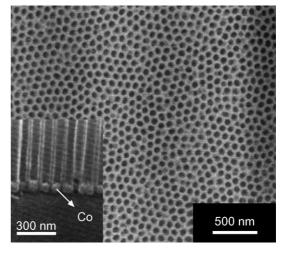

Fig. 1. Top-view SEM image of the nanoporous AAO film after pore widening in a 5% H_3PO_4 solution for 60 min. The inset is a cross-sectional view of the AAO film after Co electroplating.

tube is shown in this figure. The multiwalled tube is composed of about 70–80 well-ordered graphitic walls and a 7-nm-wide hollow core. The interwall distance (d_{002}) is approximately 3.6 Å, which is larger than the interplanar separation of graphite (d_{002}=3.35 Å). The larger interwall distance results from the curvature of the graphitic walls. The inset in Fig. 3 shows that a Co catalyst particle is

encapsulated at the tip of tube and covered by graphitic cap, indicating that the CNT growth is Co-catalyzed and by means of the tip-growth mechanism [22,23].

While the Co-catalyzed CNTs are grown on the AAO template, the nanotube growth and the carbon deposition on the AAO pore wall take place simultaneously [24]. As shown in Fig. 2c, the AAO surface appears to be covered with a thin layer of carbonaceous sediment, which blocks the outgrowth of most CNTs. In order to investigate the chemical nature of carbon in the nanotube and the sediment, Auger electron spectroscopy (AES) analyses were performed. Fig. 4 shows the carbon (KVV) Auger signals of the AAO templated CNTs and the deposited films on the AAO surface. By carefully analyzing the carbon (KVV) Auger line shape, one can obtain qualitative insight into the bonding structure of carbon atoms in carbon-based materials such as diamond, graphite, and amorphous carbon [25]. The carbon Auger signal shown in Fig. 4a with a peak situated near 260 eV indicates that the carbon of CNT produced in this study is predominantly well-crystallized sp^2-bonded (crystalline graphite-like). For the area covered by the carbonaceous sediment, the KV_2V_3 trough located at 258 eV becomes vague (see Fig. 4b and c), implying that the films mainly consist of amorphous carbon. These amorphous carbon layers, which are the byproduct of the CNT growth, are formed by the plasma decomposition of CH_4 and H_2 gases and condensed on the AAO surface. As the synthesis continues, it will gradually cover up the AAO nanopores and prevent the nanotubes from growing out of the nanopores. Therefore, in this study, the amorphous carbon
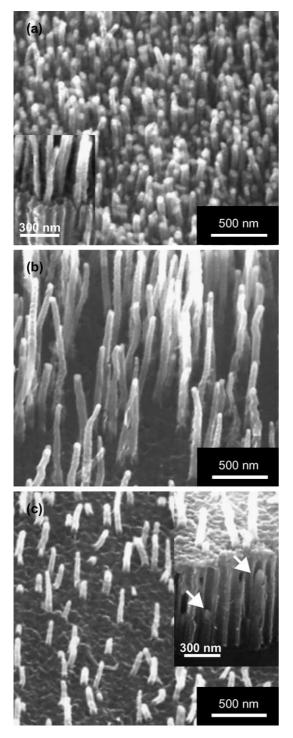

Fig. 2. Side-view SEM images of the Co-catalyzed CNTs on AAO template grown at CH_4 concentrations of (a) 9%, (b) 50%, and (c) 91%. The insets show the close-up view of the CNTs grown out of the AAO nanopores.
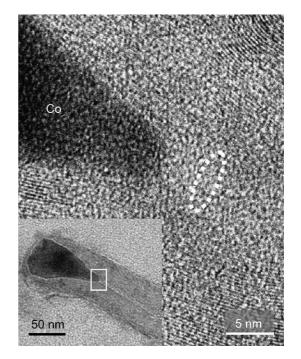

Fig. 3. HRTEM image of a Co-catalyzed CNT shown in Fig. 2b. The hollow core is indicated by a dashed ellipse. The inset is a corresponding low magnification TEM image. The square presents the magnified area of the HRTEM image.
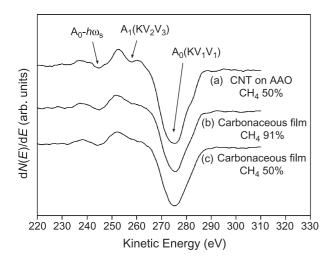
Fig. 4. Graphitic Auger carbon (KVV) peaks of (a) an AAO-assisted CNT grown at 50% CH_4, (b) the deposited carbonaceous film on the AAO surface grown at 91% CH_4, and (c) 50% CH_4.

byproduct seems to play an important role in the control of the tube number density of CNTs grown on the AAO template.

Fig. 5 shows Raman spectra of the samples shown in Fig. 2. All spectra show two prominent bands located at approximately 1330 (D band) and 1590 cm^{-1} (G band). The G band relating to the vibration of sp^2-bonded carbon atoms in a two-dimensional hexagonal lattice indicates the presence of crystalline graphitic carbon atoms [26]. The D band originates from vibrations of carbon atoms with dangling bonds in plane terminations of disordered graphite or glassy carbons. In general, the intensity of the D band increases with an increase in the amount of unorganized carbon in samples or a decrease in graphite crystal size [27]. The ratio of the integral intensities of the D and G bands, I_D/I_G, in this case is estimated as an indication of the deposition amount of the amorphous carbon byproduct. In Fig. 5, it is found that the I_D/I_G ratio increases significantly
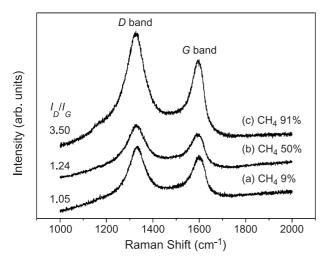
with increasing the CH_4 concentration, suggesting that the amount of amorphous/disordered carbon atoms increases markedly as the CH_4/H_2 feed ratio increases [28]. This phenomenon is in agreement with the SEM observations shown in Fig. 2 and correlates closely with the etching effect induced by H_2 in plasma. During the CNT growth in the CH_4/H_2 plasma, the amorphous carbon byproduct is deposited on the substrate surface, whereas reactive hydrogen species in the plasma can also etch away the amorphous byproduct simultaneously [29]. If a high H_2 concentration is used, the substrate surface would almost free from the amorphous carbon since it is quickly etched away by the hydrogen species. In contrast, if a high CH_4 concentration is used, the amorphous carbon deposition predominates over the etching action, resulting in the continuing growth of the amorphous carbon. This eventually leaves the substrate surface covered with an amorphous carbon layer, as shown in Fig. 2c. A considerably high I_D/I_G ratio of about 3.50 was detected for the growth condition of 91% CH_4.

The CH_4/H_2 flow ratio of the gas precursor decisively affects not only the deposition of the amorphous carbon byproduct but also the growth rate of CNTs. As clearly seen in Fig. 2, after the CNT growth for 30 min, the nanotubes grown at a CH_4 concentration of 91% are obviously shorter than that grown at 50% and 9%. Fig. 6 plots the overgrown tube length from the AAO surface against the CH_4 and H_2 concentrations. Increasing the CH_4 content tends to reduce the tube length. However, for CNT growth with the CH_4 concentrations below 50%, the obtained tube lengths depend weakly on the CH_4 concentration. This is due to that after the CNTs were grown to these lengths/ the activation of the Co catalyst was probably lost and the CNT growth was terminated. Even if the growth time was increased further, the nanotubes did not grow anymore. Here, we propose a possible mechanism for the reduction of the tube growth rate. It is well known that the H_2 content in
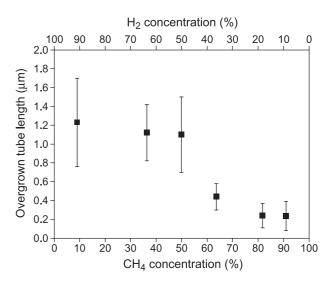

Fig. 5. Raman spectra of the AAO-assisted CNTs grown at (a) 9% CH_4, (b) 50% CH_4, and (c) 91% CH_4. The labeled value of I_D/I_G ratio is estimated in terms of the integral intensity.

Fig. 6. Overgrown tube length from the AAO surface as a function of CH_4 and H_2 concentration.
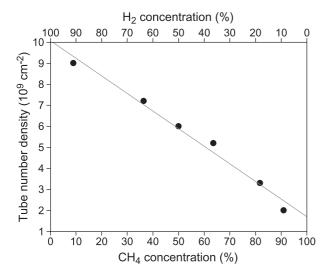
Fig. 7. Tube number density of CNTs overgrown from AAO template as a function of CH_4 and H_2 concentration.

the plasma can effectively promote the decomposition of CH_4 gas [30]. During the CNT growth, carbonaceous reactive species needed for CNT growth, such as CH_4 radicals, can be generated by hydrogen abstraction reactions [31] and then decomposed by the transition metal catalyst. These reactive species will eventually initiate the formation of CNTs. A large content of H_2 in the plasma can efficiently decompose the CH_4 gas, resulting in a large amount of the carbonaceous reactive species and thus a high CNT growth rate. Therefore, in our results, the tube growth rate was decreased significantly following the increase of the CH_4/H_2 feed ratio, which is essentially a consequence of decreasing the CH_4 decomposition efficiency. Besides, in the growth condition of a high CH_4/H_2 ratio, the large amount of amorphous carbon sediment may also be deposited on the CNT tip, which will hinder the diffusion of carbonaceous reactive species to the Co catalyst and consequentially reduce the tube growth rate.

The density control of CNTs grown on the AAO template can be achieved by directly tuning the CH_4/H_2 feed ratio during the CNT growth. When a high CH_4/H_2 feed ratio is used, the deposition of the amorphous carbon byproduct proceeds quickly and the CNT growth is retarded in terms of the tube length as indicated in Fig. 6, causing that most nanotubes are blocked inside the nanopores by the amorphous carbon sediment and unable to grow out. As shown in the inset of Fig. 2c, some short nanotubes marked by white arrows were buried inside the nanopores. Nevertheless, the CNTs, which have already sprouted out of the nanopores, can continuously grow since the CNT growing site is at the tip of the tubes (tip-growth mechanism). With a high CH_4 concentration of 91%, only about 18% of CNTs could grow out from the nanopores. On the other hand, in a low CH_4/H_2 feed ratio, the AAO surface is almost free from the amorphous carbon (see the inset of Fig. 2a) because the etching effect caused by hydrogen species is dominant, and CNTs can grow fast, leading to a very high tube number

density. In this context, the number of CNTs grown over the AAO nanopores is strongly influenced by the CH_4/H_2 feed ratio. Fig. 7 plots the tube number density of CNTs overgrown from the AAO template as a function of the CH_4 and H_2 concentrations. It nearly presents a inverse proportional relation between the tube number density and the CH_4 concentration. The tube density decreased 4.5 times in magnitude, and the corresponding tube filled ratio in the AAO nanopores decreased from 82% to 18%, when the CH_4 concentration increased from 9% to 91%.

4. Conclusions

We report a simple and reliable method to control the tube number density of aligned CNTs grown on the nanoporous AAO template. The key idea of this method is to take advantage of the competition between the growth of Co-catalyzed CNTs from the AAO pore bottom and the deposition of the amorphous carbon byproduct on the AAO nanoporous template. The number of CNTs grown over the nanopores is strongly depended on the flow rate ratio of CH_4 and H_2 in the precursor gas mixture during the CNT growth. It was found that the tube density of the CNT arrays on the AAO template decreases linearly with increasing the CH_4 concentration. By adjusting the CH_4/H_2 feed ratio, one can control the percentage of nanotubes overgrown out of the AAO nanopores from 82% to 18%.

References

[1] S. Iijima, Nature 354 (1991) 56.
[2] W.A. de Heer, A. Chatelain, D. Vagaret, Science 270 (1995) 1179.
[3] Yahachi Saito, Sashiro Uemura, Carbon 38 (2000) 169.
[4] Niels de Jonge, Yann Lamy, Koen Schoots, Tjerk H. Oosterkamp, Nature 420 (2002) 393.
[5] J. Li, C. Papadopoulos, J.M. Xu, M. Moskovits, Appl. Phys. Lett. 75 (1999) 367.
[6] Jung Sang Suh, Jin Seung Lee, Appl. Phys. Lett. 75 (1999) 2047.
[7] Z.H. Yuan, H. Huang, H.Y. Dang, J.E. Cao, B.H. Hu, S.S. Fan, Appl. Phys. Lett. 78 (2001) 3127.
[8] Eun Ju Bae, Won Bong Choi, Kwang Seok Jeong, Jae Uk Chu, Gyeong-Su Park, Seahn Song, In Kyeong Yoo, Adv. Mater. 14 (2002) 277.
[9] A.P. Li, F. Müller, A. Birner, K. Nielsch, U. Gösele, J. Appl. Phys. 84 (1998) 6023.
[10] O. Jessensky, F. Müller, U. Gösele, Appl. Phys. Lett. 72 (1998) 1173.
[11] Takashi Kyotani, Li-Fu Tsai, Akira Tomita, Chem. Mater. 8 (1996) 2109.
[12] Y.C. Sui, D.R. Acosta, J.A. González-León, A. Bermúdez, J. Feuchtwanger, B.Z. Cui, J.O. Flores, J.M. Saniger, J. Phys. Chem., B 105 (2001) 1523.

[13] Jin Seung Lee, Geun Hoi Gu, Hoseong Kim, Kwang Seok Jeong, Jiwon Bae, Jung Sang Suh, Chem. Mater. 13 (2001) 2387.

[14] Soo-Hwan Jeong, Ok-Joo Lee, Kun-Hong Lee, Chem. Mater. 14 (2002) 1859.

[15] L. Nilsson, O. Groening, C. Emmenegger, O. Kuettel, E. Schaller, L. Schlapbach, H. Kind, J.-M. Bonard, K. Kern, Appl. Phys. Lett. 76 (2000) 2071.

[16] Z.F. Ren, Z.P. Huang, D.Z. Wang, J.G. Wen, J.W. Xu, J.H. Wang, L.E. Calvet, J. Chen, J.F. Klemic, M.A. Reed, Appl. Phys. Lett. 75 (1999) 1086.

[17] Shoushan Fan, Michael G. Chapline, Nathan R. Franklin, Thomas W. Tombler, Alan M. Cassell, Hongjie Dai, Science 283 (1999) 512.

[18] Y. Tu, Z.P. Huang, D.Z. Wang, J.G. Wen, Z.F. Ren, Appl. Phys. Lett. 80 (2002) 4018.

[19] Soo-Hwan Jeong, Ok-Joo Lee, Kun-Hong Lee, Sang-Ho Oh, Chan-Gyung Park, Chem. Mater. 14 (2002) 4003.

[20] H. Masuda, K. Fukuda, Science 268 (1995) 1466.

[21] Po-Lin Chen, Cheng-Tzu Kuo, Tzeng-Guang Tsai, Bo-Wei Wu, Chiung-Chih Hsu, Fu-Ming Pan, Appl. Phys. Lett. 82 (2003) 2796.

[22] R.T.K. Baker, Carbon 27 (1989) 315.

[23] Stig Helveg, Carlos López-Cartes, Jens Sehested, Poul L. Hansen, Bjerne S. Clausen, Jens R. Rostrup-Nielsen, Frank Abild-Pedersen, Jens K. Nørskov, Nature 427 (2004) 426.

[24] Soo-Hwan Jeong, Hee-Young Hwang, Kun-Hong Lee, Yongsoo Jeong, Appl. Phys. Lett. 78 (2001) 2052.

[25] P.G. Lurie, J.M. Wilson, Surf. Sci. 65 (1977) 476.

[26] A. Kasuya, Y. Sasaki, Y. Saito, K. Tohji, Y. Nishina, Phys. Rev. Lett. 78 (1997) 4434.

[27] R.J. Nemanich, S.A. Solin, Phys. Rev., B 20 (1979) 392.

[28] A.C. Ferrari, J. Robertson, Phys. Rev., B 61 (2000) 14095.

[29] O.M. Kuttel, O. Groening, C. Emmenegger, L. Schlapbach, Appl. Phys. Lett. 73 (1998) 2113.

[30] Young Chul Choi, Dong Jae Bae, Young Hee Lee, Byung Soo Lee, Gyeong-Su Park, Won Bong Choi, Nae Sung Lee, Jong Min Kim, J. Vac. Sci. Technol., A, Vac. Surf. Films 18 (2000) 1864.

[31] Thanh N. Truong, J. Chem. Phys. 100 (1994) 8014.